Cancer immunotherapy response persists after lymph node resection

Hengbo Zhou[1,2#], Lutz Menzel[1#], James W. Baish[3], Meghan J. O'Melia[1], Laurel B. Darragh[4], Derek N. Effiom[5], Emma Specht[5], Juliane Czapla[5], Pin-ji Lei[1], Johanna J. Rajotte[1], Lingshan Liu[1], Mohammad R. Nikmaneshi[1], Mohammad S. Razavi[1], Matthew G. Vander Heiden[2,6], Jessalyn M. Ubellacker[7], Lance L. Munn[1], Sana D. Karam[4], Genevieve M. Boland[5], Sonia Cohen[5] and Timothy P. Padera[1]

[1] Edwin Steele Laboratories, Department of Radiation Oncology, Massachusetts General Hospital

[2] Koch Institute for Cancer Research and Department of Biology, Massachusetts Institute of Technology

[3] Department of Biomedical Engineering, Bucknell University

[4] Department of Radiation Oncology, University of Colorado Anschutz Medical Campus

[5] Department of Surgery, Massachusetts General Hospital

[6] Department of Medical Oncology, Dana-Farber Cancer Institute

[7] Department of Molecular Metabolism, Harvard T.H. Chan School of Public Health

[#] Authors contributed equally

Abstract

Lymphatic transport facilitates the presentation of cancer antigens in tumor-draining lymph nodes (tdLNs), leading to T cell activation and the generation of systemic antitumor immune surveillance. Surgical removal of LNs to control cancer progression is routine in clinical practice. However, whether removing tdLNs impairs immune checkpoint blockade (ICB) is still controversial. Our analysis demonstrates that melanoma patients remain responsive to PD-1 checkpoint blockade after LN dissection. We were able to recapitulate the persistent response to ICB after complete LN resection in murine melanoma and mammary carcinoma models. Mechanistically, soluble antigen and antigen-carrying migratory dendritic cells are diverted to non-directly tumor draining LNs (non-tdLNs) after tdLN dissection. Consistently, robust ICB responses in patients with head and neck cancer after primary tumor and tdLN resection correlated with the presence of reactive LNs in distant areas. These findings indicate that non-tdLNs sufficiently compensate for the removal of direct tdLNs and sustain the response to ICB.

Introduction

Advances in our understanding of the mechanisms of T cell activation and exhaustion led to the identification of several immune checkpoints, such as programmed death 1 (PD-1)[1,2] and cytotoxic T lymphocyte antigen 4 (CTLA-4)[3,4], which are now therapeutic targets[5,6]. Immune checkpoint blockade (ICB) has been approved for the treatment of many cancers, including melanoma[7,8] and breast cancer[9,10]. However, an improved understanding of the mechanisms of ICB therapy is necessary to benefit more patients. Lymph nodes (LNs) surveil tissue fluids and initiate adaptive immunity[11]. Due to the direct drainage of interstitial fluid and tumor-derived cells to lymph nodes by lymphatic vessels within the lymphatic drainage region (lymphosome), metastatic dissemination to tumor-draining lymph nodes (tdLNs) can occur during the early stage of tumor growth[12]. Colonization in LNs often impairs nodal entry of naïve lymphocytes[13], causes expansion of regulatory T cells (Tregs)[14–16] and induces systemic tolerance in favor of cancer progression[15]. LN metastases can also disseminate to distant metastatic sites[17,18], further driving cancer progression.

Sentinel lymph node biopsy (SLNB) and completion lymph node dissection (CLND) are commonly performed[19–23] to assess the disease stage and to limit cancer progression. Seminal work demonstrated that tumor-specific T cells and non-exhausted tumor-specific memory T cells are enriched in tumor-draining, but not in other LNs[24,25], suggesting that removal of tdLNs would impair anti-cancer immune responses. However, in a phase III clinical trial, melanoma patients treated with tumor, sentinel LN and metastatic LN resection still responded to anti-CTLA4 therapy, indicating that the presence of tdLNs may not be necessary to maintain ICB efficacy[26]. Similarly, administering anti-CTLA4 locally to the lymphatic basin at the site of the resected tumor enhanced effector T cell activation, lasting up to 3 months after SLNB. This suggests that the ICB-mediated immune response extends beyond just the sentinel LNs[27]. Due to the important role of LNs in the adaptive immune response, it is imperative to evaluate the effects of SLNB and CLND on ICB efficacy. Our retrospective analysis demonstrates that stage III melanoma patients with SLNB, and surprisingly even CLND benefit from adjuvant anti-PD1 inhibition. Using orthotopic breast cancer and melanoma models in mice, we were able to show that ICB efficacy persists after tdLN dissection as a result of a compensatory mechanism by which tumor-derived antigen and migratory dendritic cells are diverted to non-directly tumor draining LNs (non-tdLNs). This phenomenon was corroborated in head and neck cancer patients who underwent neoadjuvant and/or adjuvant ICB therapy and bilateral neck dissection, where the ICB response was associated with the presence of reactive LNs at distant sites. To apply our findings to improve treatment stategies, we compared systemic versus locoregional administration and found that delivering ICB to the lymphosome of reactive non-tdLNs improves anti-tumor T cell responses after CLND.

Results

Stage III patients with melanoma respond to ICB after CLND. Prior to the availability of effective systemic therapies for patients with melanoma, LN surgery played a major role in the treatment of patients with locoregional disease. Any patient with clinically evident LN metastases or a positive SLNB underwent CLND for disease control. In 2017, MSLT-II[28] (a randomized clinical trial of CLND vs observation in early-stage melanoma patients with a positive SLNB) demonstrated that CLND did not improve melanoma-specific survival (MSS). Due to the morbidity associated with CLND, this trial led to a change in clinical practice, favoring observation for early-stage patients with melanoma with a positive SLNB. CLND is now reserved for cases of disease recurrence in the draining LN basin. Approximately 20% of patients will eventually experience recurrence in the draining nodal basin, while 80% of patients with a positive SLNB will thus be spared the unnecessary morbidity risk of CLND[28].

Given the importance of tdLNs for ICB response in mouse models[25,29,30] and humans,[31] we asked whether the extent of LN surgery impacts the effectiveness of ICB treatment. Our retrospective analysis included 66 patients with stage III melanoma treated with surgery and adjuvant anti-PD1 therapy (nivolumab or pembrolizumab), from which 16 underwent CLND and 50 underwent only SLNB (**Figure S1A**). Surprisingly, there was no statistically significant difference in melanoma specific survival (MSS) (**Fig. 1A**) or recurrence-free survival (RFS) (**Fig. 1B**) between both groups. Furthermore, no significant differences were observed after stratification by local recurrence-free survival (**Fig. 1C**) and distant recurrence-free survival (**Fig. 1D**). To validate these findings in patients with metastatic disease in the tdLN basin, we narrowed our cohort to patients with a positive SLNB (**Figure S1A**). Of note, the number of patients undergoing CLND is minimal (**Figure 1B**) as a result of the MSLT-II trial findings—which demonstrated that CLND provided no (MSS) benefit.[28] We selected stage IIIC patients to assess whether the extent of nodal surgery in patients with known metastatic melanoma in the draining nodal basin affected the response to anti-PD1 therapy (**Figure 1C-E**). Anti-PD1 therapy significantly enhanced the RFS in patients who did not undergo lymph node surgery, consistent with clinical trial data (**Fig. 1E)**. However, LN dissection did not impair the efficacy of anti-PD1 treatment (**Fig. 1E**). These findings were confirmed in a recently reported retrospective analysis of sentinel LN positive, stage III melanoma patients treated with adjuvant anti-PD-1 monotherapy that underwent CLND or no LN dissection. Multivariate analysis of 261 patients from 39 independent institutions receiving adjuvant anti-PD-1 treatment showed no difference in 2-year overall survival (OS) or RFS with or without CLND (2-year RFS: 55.9% vs. 52.6%, p=0.74; 2-year OS: 83.4% vs. 83.6%, p=0.73)[32]. These data demonstrate that the response to ICB persists in patients after SLNB and CLND surgery.

ICB response persists after tdLN dissection in mice. To determine if the sentinel LNs or a combination of the sentinel LN and adjacent LNs are required for efficacy of ICB response, we orthotopically implanted murine melanoma cells (intradermal injection of B16F10 or YUMMER1.7), or murine breast cancer cells (mammary fat pad injection of E0771). According to the timeline outlined in recent studies[25,29], which involved administering three doses of IgG or anti-PD1 treatment every 2 days starting on day 7 after orthotopic cancer cell implantation, micrometastases in LNs were detected on day 13 in both IgG- and ICB-treated mice. However, larger metastases were observed in IgG treated animals (**Figure S2A)**. To test whether removal of tdLNs alters ICB response in the three cancer models, we performed sham surgeries, surgically removed the ipsilateral inguinal (SLNB) or surgically removed a combination of the ipsilateral inguinal (inLN), axillary (axLN), and brachial (brLN) LNs (CLND) 6 days after orthotopic tumor implantation. Subsequent treatment with anti-PD1 antibody (3 doses of anti-PD-1 starting day 7, every 2 days for B16F10 and YUMMER1.7 tumors or every 3 days for E0771 tumors) resulted in a significant tumor growth delay for E0771 and YUMMER1.7 tumors (**Figure S2B**) and increased the survival in all three tumor models compared to IgG controls (**Fig. 2A**).

To determine whether 6 days of priming the tdLNs was sufficient to generate systemic anti-cancer immunity, we used pre-emptive LN removal similar to that used in recent studies.[25,29] We performed SLNB or CLND before tumor implantation and again found that LN resection has no negative effect on ICB response (**Fig. 2B**). The frequency of complete responders (CR) with anti-PD1 treatment was similar to IgG controls in the weakly-immunogenic B16F10 tumor model, but showed significant differences in the moderately-responsive E0771 and responsive YUMMER1.7 tumor models (**Fig. 2C**). The extent of LN surgery did not alter the frequency of CRs in anti-PD-1 treated animals in any of the tumor models tested. (**Fig. 2C**). These findings are not consistent with recent investigations using MC38 and CT26 tumor models grown ectopically in the subcutaneous setting.[25,29] When E0771 was implanted ectopically in the dermis, CLND was able to reduce the response to anti-PD1 (**Figure S2C, D**), indicating altered immune response can occur when tumor cells are implanted ectopically.

These findings prompted us to examine whether LNs are even necessary for ICB efficacy. *Lta*$^{-/-}$ mice, which do not form mature inguinal, brachial, axillary and popliteal (among other) LNs while maintaining other parts of the lymphatic system[33–35], were orthotopically implanted with B16F10 and E0771 tumors and treated with ICB. Tumors grew more rapidly in *Lta*$^{-/-}$ mice compared to wild-type mice (**Figure S2E**), showing the importance of LNs in tumor control. In contrast to wildtype (WT) mice, however, PD1 inhibition did not affect tumor growth or overall survival in *Lta*$^{-/-}$ mice (**Figure S2E**), suggesting that effective ICB treatment requires LNs in general, but not the direct tdLNs. These results indicate LN-dependent compensatory mechanisms occur after CLND to maintain ICB response.

Removal of draining LNs promotes antigen transport to distant LNs. To interrogate these compensatory mechanisms, we injected surrogate antigens (fluorophore-conjugated dextran of 4.4 kDa or 2,000 kDa) into the 4th mammary fat pad (MFP) to measure the local and systemic transport to alternative lymph nodes after SLNB or CLND. Most of the 2,000 kDa dextran aggregated in the LN subcapsular sinus (SCS) (**Fig. 3A**) and appeared within lymphatic vessels of the LN medulla (**Fig. 3B**) confirming that molecules of this size are predominantly transported via lymph flow. 4.4 kDa dextran entered the LN parenchyma and were distributed throughout the paracortex (**Fig. 3A**), consistent with entry via blood or lymph. Small biomolecules are known to access the blood circulation, whereas molecules larger than 40 kDa transport more through lymph and are retained within the SCS when they arrive in the LN[36]. Six hours after injection, the abundance of 2,000 kDa dextran in axillary LNs (axLNs) after resection of the draining inLN (SLNB) is similar to the inLN under sham conditions. Minimal 2,000 kDa dextran was detected in contralateral LNs after SLNB. Surprisingly, 2,000 kDa dextran was detected in the contralateral inLN six hours post-injection after CLND (**Fig. 3C**), showing a distant diversion of the dextran.

To further test whether antigen access to distant LNs can be enhanced when local lymphatic drainage is ablated, we dissected the popliteal LN (poLN), inLN, axLN and brachial LN (brLN) of the ipsilateral side (ILND) and injected the dextran into the ipsilateral foot pad. Avoiding injection-induced lateral flow of antigen by food pad injection allowed us to monitor compensatory lymph drainage after ILND. Similar to results in **Fig. 3A**, we discovered that the 2,000 kDa dextran was mainly located within the ipsilateral poLN, inLN and axLNs when lymphatic drainage was intact (sham), whereas ILND diverted the lymph transport to the contralateral inLN and axLN (**Figure S3A, B**). The absence of 2,000 kDa dextran in the contralateral poLNs suggests that, once taken up by lymphatic vessels of an adjacent lymphosome, lymph-borne antigens follow normal drainage patterns and do not undergo retrograde flow or circulate significantly through the blood. In contrast, 4.4 kDa dextran was found in all of the remaining LNs (**Figure S3A, B**), suggesting transport through lymph and blood that results in a systemic distribution. The compensatory drainage phenomenon suggested by our data has also been reported clinically, including evidence that lower limb interstitial fluid can cross the lower abdomen towards the contralateral inguinal region[37–39]. Corresponding to these reports, we tested if the interstitial transport from a disrupted lymphosome crosses the midline and reaches contralateral LNs using a dermal route. We surgically cut the skin along the midline (lower abdomen to chest) in CLND mice to interrupt intradermal transport, and then injected dextran into the ipsilateral MFP. Dextran transport to contralateral LNs was detected in mice with intact midline skin but was absent after midline incision **(Fig. 3D)**. This data indicates that interstitial fluid can move across the midline through the dermis and reach an adjacent lymphosome draining to distant LNs after CLND. In addition to distant LNs, we detected higher abundance of the 2,000 kDa dextran in spleens of mice with CLND, compared to sham mice (**Fig. 3E**). The 2,000 kDa dextran molecules were primarily located within and around the B cell follicles and phagocytized by adjacent macrophages (**Fig. 3E**). In summary, after removal of the primary dLN (SLNB) antigen moves through interstitial tissues to the edge of an adjacent lymphosome

with intact lymphatic drainage, where the antigen is taken into initial lymphatic vessels and follows the normal lymphatic drainage to the associated LN. Through this mechanism, antigen is able to cross the midline to contralateral LNs after CLND (**Fig. 3F**).

Mathematical modeling shows antigen access to adjacent lymphosomes via dermal interstitial transport after TDLN dissection. Our data show that interstitial antigen enters adjacent lymphosomes after dissection of one or more LNs (**Fig. 3**). On this basis, we developed anatomically-based, computational models of lymph flow rates to LNs and interstitial fluid pressure (IFP) that predict how antigens and large tracer molecules can be redistributed when superficial lymphosomes are disabled by removing their draining lymph nodes. The models recapitulate our primary experimental findings in mice (**Fig. 4A-F**) and predict how these results may translate to clinical practice in humans (**Fig. 4G-I**). Details of the model are provided in **Supplemental Materials** along with analytical validation and parametric studies.

The color maps in **Fig. 4C-F, I** show how disabling various combinations of the inLN, axLN, brLN and poLN causes local increases in interstitial fluid pressure that divert fluid lost from blood capillaries to adjacent lymphosomes where it can be absorbed by active lymphatic vessels. The size of the black circles in **Fig. 4C-F, I** indicates the fractional increase in flow to other lymph nodes when selected lymph nodes were disabled. Normally, an equilibrium exists in which fluid lost from the blood capillaries is absorbed by a highly-connected network of valve-less, noncontracting initial lymphatic vessels and then actively pumped to local lymph nodes via collecting lymphatic vessels. Under normal conditions, interstitial fluid pressures remain at or slightly below atmospheric pressure with little lateral movement of fluid occurring in the superficial tissue layers. In contrast, when local lymph nodes were computationally removed, accumulating fluid increases the local interstitial pressure inducing passive flow through the dermal initial lymphatic vessels and dermis from regions of high interstitial pressure to distal regions with intact lymph nodes where the interstitial pressure remains at its normal, low level. Typically, disabling a lymph node changed the flow most significantly in adjacent lymphosomes, although flow was also perturbed farther away. **Fig. 4F** shows that numerically severing the skin flow along the midline prevents flow changes on the contralateral side as we observed experimentally (**Fig. 3D**).

Our results in a human model (**Fig. 4G-I**) were qualitatively similar to those in mice, but important differences arise because of the relative size of the lymphosomes, anatomical connectivity of the vessels, and the degree of redundancy in the human lymphatic networks. When compared to the large lymphosomes found in humans, the small lymphosomes found in mice drain smaller quantities of fluid over shorter distances and generate only modest increases interstitial pressure when a LN is disabled. For example, compare the low IFP (light blue) in **Fig. 4C** for a disabled inguinal node in a mouse to the much higher IFP (red) at the center of the human chest when axillary drainage is disabled in **Fig. 4I**. This size difference alone may account for much of the relative difficulty in creating experimental models of lymphedema in laboratory mice.

To further examine the effect of anatomical size, we compared the IFP in the skin from the human 3D model with an analytical assumption of a planar, circular lymphosome with equal surface area and found that both models resulted in similar distribution patterns of IFP relative to lymphosome size (**Figure S4A, B**). To examine the size dependence of lymphosomes, we performed a parametric study of the model and found that larger lymphosomes, such as those found in humans, collect a higher volume of interstitial fluid resulting in higher IFP, which then maintains higher lymph flow (**Figure S4C**). The model demonstrates how the mobility of the fluid (κ) in the superficial network of initial lymphatic

vessels affects the IFP but has little influence on the total quantity of antigen-carrying fluid diverted elsewhere from its initial destination (**Figure S4D**). The similar lymph fluid diversion patterns and transport to compensatory LNs between the experimental mouse model and the mathematical model of human antigen drainage suggests our results are relevant for predicting lymph drainage in patients with or without LN dissection. The greater number of lymph nodes in the axillary and inguinal regions in humans compared to mice also alters the likely effects of removing any single lymph node.

Tumor antigen-carrying and presenting DCs elicit T cell responses in non-tdLNs after CLND. Knowing that interstitial antigens are drained by contralateral LNs after CLND, we tested if tissue-resident DCs take up particles in the primary tumor and migrate to these compensatory LNs. $B16^{OVA-zsGreen}$ tumors implanted in mice treated with LN surgery and ICB therapy (**Figure S5A**) grew significantly slower in the anti-PD1 group with no detrimental effect of CLND (**Fig. 5A**). Flow cytometry analysis (**Figure S5B**) revealed a significant increase of migratory DCs in tdLNs on the ipsilateral side after sham surgery and in contralateral LNs after CLND, while contralateral LNs after sham surgery were similar to LNs from tumor-naïve controls (**Fig. 5B**). To test the premise that DCs take up tumor-derived antigens, the fluorescent protein zsGreen from tumors cells was used. zsGreen was detected in all tumor cells and a majority of DCs within the primary tumor (**Figure S5C**). We also found high numbers of $zsGreen^+$ DCs in the ipsilateral draining LNs while very few $zsGreen^+$ DCs were found in contralateral LNs after sham surgery. In contrast, $zsGreen^+$ DCs were present in contralateral LNs after CLND (**Fig. 5C**). We confirmed these findings by staining for DCs presenting ovalbumin antigen (MHC-I:SIINFEKL), showing significantly more SIINFEKL-presenting DCs within the ipsilateral LNs of sham surgery mice and contralateral LNs of CLND mice (**Figure S5D**). While $zsGreen^+$ DCs show a clear predominance in LNs compared to the spleen, $zsGreen^+$ macrophages were increased in the spleen after CLND, in line with our observation of $FITC^+$ macrophages in the spleen after dextran injection (**Figure S5E, F**). In agreement with previous reports[40], the numbers of $zsGreen^+$ LN-resident DCs were approximately 10-fold higher than $zsGreen^+$ migratory DCs (**Fig. 5D**). Our data indicate that interstitial antigens and antigen-carrying migratory DCs both reach the contralateral LN after CLND but LN-resident DCs are likely dominant in presenting tumor antigens.

We next examined whether T cell responses are generated in non-tdLNs after CLND. After $B16^{OVA-zsGreen}$ implantation, ipsilateral LNs from sham surgery mice and contralateral LNs from CLND mice had significant cellular expansion (**Figure S5G**) and contained more CD8 T cells (**Fig. 5E**). Concomitantly, the number of antigen-experienced ($CD44^+PD1^+$) T cells was significantly higher in ipsilateral LNs from sham surgery mice and contralateral LNs from CLND mice with the numbers further increasing with anti-PD1 treatment after CLND (**Fig. 5F**). We confirmed the previous results of DCs presenting tumor-antigen and T cell priming in contralateral LNs after CLND by performing ipsilateral food pad injection of bone marrow-derived DCs (BMDCs) that were pulsed with OVA and stimulated with lipopolysaccharide (LPS) *in vitro* prior to injeciton. OVA-$tetramer^+$ T cells (referred to as OVA-T cells) were significantly enriched in ipsilateral LNs of sham mice and contralateral LNs of CLND mice (**Figure S5H**), suggesting that antigen-carrying DCs migrate to distant LNs and successfully elicit T cell responses specific to the carried antigen. OVA-T cells were also enriched during $B16^{OVA-zsGreen}$ tumor growth in ipsilateral LNs of sham mice and contralateral LNs of CLND mice but were almost non-existent in contralateral or cervical LNs of sham mice (**Fig. 5G**), emphasizing that CLND induces regional redistribution of antigen but not systemic antigen diversion. The abundance of OVA-T cells was similar in spleens and blood of sham and CLND mice after anti-PD1 treatment (**Fig. 5h**), demonstrating that the generation of circulating tumor-specific T cells persists after LN surgery.

We further tested the T cell response in an adjuvant setting. We resected primary tumors in combination with sham or CLND surgery, followed by subsequent anti-PD-1 treatment. There was no difference in abundance of OVA-T cells between ipsilateral LNs from sham surgery mice and contralateral LNs from CLND mice (**Fig. 5I**), indicating that even without the primary tumor as a source of antigen, non-tdLNs are able to generate tumor-specific T cell responses. In addition to T cell responses in LNs, we analyzed primary tumor-infiltrating T cells and found that anti-PD1 treatment enhanced proliferating effector T cells in sham and CLND mice (**Fig. 5J**, **Figure S6A**). Moreover, adjuvant anti-PD1 treatment of sham and CLND mice induced the generation of a memory T cell population in newly implanted tumors. Non-exhausted stem-like central memory CD8 T cells were similarly abundant in ipsilateral LNs of sham mice and contralateral LNs of CLND mice (**Fig. 5K**, **Figure S6B**). Using photoconversion of the contralateral LN in Kaede mice after rechallenge with $B16^{OVA\text{-}zsGreen}$ tumors, we confirmed that tumor-specific T cells from non-tdLNs traffic to recurrent tumors after CLND (**Fig. S6C**). Taken together, ICB-mediated expansion of tumor-infiltrating T effector and T memory cells persist after CLND.

Spleens have a minor compensatory effect for ICB treatment after LN resection. Our data indicate that large dextran molecules can access the spleen after sham and CLND surgery (**Fig. 3E**), accompanied by a tumor-specific T cell response (**Fig. 5H**). We next tested whether the spleen is essential for maintaining an ICB response in mice after CLND. Sham surgery or splenectomy (SpX) were performed 2 weeks prior to CLND. After 10 days of recovery, E0771 tumors were implanted and then treated with ICB on days 7, 10 and 13 after implantation (**Figure S7A)**. The splenectomy did not affect the overall survival in CLND mice treated with anti-PD-1. Complete responders were less frequent, but still present in mice with SpX (**Figure S7A**). Further, all complete responders (5/5) from sham and 2 out of 3 SpX mice rejected tumors after rechallenge (**Figure S7B**), showing the generation of immune memory in SpX mice. Altogether, these data suggest that the spleen only marginally contributes to ICB responses after CLND.

Administration of ICB to non-tdLNs enhances the efficacy after tdLN dissection. Previous studies demonstrated that locoregional ICB augments cancer immunotherapy[27,41,42]. These findings, together with our results, emphasize the potential of non-tdLNs as ICB target sites. Because non-tdLNs are almost only reached by tumor antigens and migratory dendritic cells after dissection of the primary tdLNs, we assessed the capacity of contralateral LNs to respond to locoregional ICB injection in mice after CLND (**Fig. 6A**). As anti-PD1 as a single target is based on a mechanism primarily effective within tumor tissue[43], we used the clinically effective combination of anti-PD1 and anti-CTLA4 treatment[44], which is more likely to have an effect during APC–T cell encounter in LNs[43]. Intradermal (*id*) administration of ICB in the lymphosome drained by the ipsilateral tdLNs with sham surgery or administration in the contralateral lymphosome in mice with CLND resulted in robust LN expansion in both groups after ICB but not in IgG treated controls (**Figure S8A**). Within the T cell compartment, ipsilateral LNs of sham mice and contralateral LNs of CLND mice shared a similar composition of T cell subsets based on principal component analysis (**Fig. 6B**), including a similar abundance of stem-like effector T cells, which are considered to be the main contributors to effective ICB responses[45] (**Fig. 6C**). To further investigate the potency of non-tdLNs for ICB treatment, we performed sham surgery or CLND in mice with E0771 tumors followed by ICB administration either intraperitoneally (*ip*) or *id* to the contralateral inLN (contra *id*). Compared to systemic administration (*ip*), contra *id* resulted in a survival benefit and a higher number of complete responders (CR) in CLND mice (**Fig. 6D**). These results suggest that delivering ICB therapeutics to non-tdLNs may benefit patients after LN surgery.

In comparison to adjuvant-only treatment, neoadjuvant-adjuvant ICB has been shown to be beneficial for patients with advanced melanoma[46]. To examine whether LN surgery compromises neoadjuvant-

adjuvant ICB efficacy, B16^{Gluc} tumors were implanted, and mice were treated with ICB delivered *id* to the tdLN followed by a curative primary tumor resection with or without LN surgery (SLNB or CLND). Mice were monitored for tumor recurrence or metastases (using Gluc activity measurement) for 100 days. All tumor-free complete responders were rechallenged with B16^{Gluc} tumors and mice that developed tumors were again treated with adjuvant ICB delivered *id* to the ipsi inLN for sham, ipsi axLN for SLNB or contra inLN for CLND (**Fig. 6E**). Interestingly, vitiligo occurred in mice after tumor/LN surgery with neo-adjuvant ICB treatment, which was primarily located at the site of surgery of the tumor resection and LN removal (**Fig. 6F**). Vitiligo indicates an ICB-induced immune response against proteins involved in melanin production beyond the melanin expressing tumor cells[47]. After neoadjuvant treatment and tumor resection, only one sham mouse developed a spontaneous tumor recurrence and one mouse of the SLNB group died due to tumor-unrelated reasons (**Fig. 6G**), demonstrating the potency of curative surgery. Upon rechallenge, all naïve control mice developed tumors, while many of the ICB-treated mice rejected the new tumor, indicating anti-tumor immune memory that was more abundant in mice with ICB treatment compared to the IgG controls. The ICB-induced immune memory and survival benefit persisted after SLNB or CLND (**Fig. 6H, I**). These results suggest that, in a LN-targeted neoadjuvant-adjuvant ICB setting, the formation of immune memory against cancer cells and improvement of overall survival persist after LN surgery and curative primary tumor resection.

LN egress of T cells is dispensable for effective anti-tumor immune memory. ICB generated complete responders in mice with sham surgery or CLND (**Fig. 2, Fig. 6**). These survivors were rechallenged with E0771 tumors at the initial tumor site, and these tumors were rejected in both groups (**Figure S8B**). We further tested whether the anti-tumor immune memory is contained only in the local tissue or is systemic. All animals rechallenged at the ipsi- and contra-lateral sides remained tumor-free (**Figure S8C**). We further found that the immune memory is tumor specific, as E0771-immune mice did not reject B16F10 tumors implanted in either the mammary fat pad or dermis (**Figure S8D**). Lymphocytes use sphingosine 1-phosphate (S1PR) as guidance cues to egress from LNs[48–50] and eventually gain access to the circulation. FTY720, a potent inhibitor of S1PR[51], drastically reduced CD4, CD8 and central memory (CD44^{+}/CD62L^{+}) CD8 T cells within the circulation (**Figure S8E)**. We aimed to test whether central memory T cells from LNs enter the circulation as contributors to the long-term immune memory in complete responders. Tumor naïve control mice or tumor-free survivors were treated with FTY720, and E0771 or B16^{Gluc} tumors were orthotopically implanted to the primary tumor site and to the contralateral site. The vast majority of ICB complete responders rejected the tumors after rechallenge regardless of the FTY720 treatment, but IgG-treated control groups demonstrated reduced tumor immunity (**Figure S8F, G**). Thus, LN surgery status did not affect the immune memory. Strikingly, the anti-tumor immune memory was not only effective in rejecting the tumor at the initial tumor implantation site, but also for tumors implanted ectopically (dermis for E0771 and mammary fat pad for B16^{Gluc}) (**Figure S8F, G)**. These findings suggest that ICB-induced anti-tumor immune memory provides systemic immunity against tumor rechallenge in complete responders while immune cells egressing from LNs are dispensable once the tumor-specific immune memory has been established. Resecting tdLNs, via SLNB or CLND after ICB treatment, had no detrimental effects on tumor rejection mediated by memory T cells.

Non-tdLNs become reactive after tumor and tdLN resection in patients treated by ICB. To test whether non-tdLNs contribute to ICB efficacy against cancer recurrence, we investigated patients from a recent phase I/Ib trial (NCT03635164)[52]. The trial included patients with HPV-negative head and neck cancer who received neoadjuvant treatment consisting of a combination of hypofractionated radiotherapy and durvalumab (targeting PD-L1). After a recovery time, patients underwent surgical resection of the primary tumor and bilateral LN dissection in the neck as standard of care. Patients with

a major or complete pathological response to neoadjuvant therapy were classified as responders (response>95%). Except for four cycles of durvalumab treatment, other adjuvant therapies (e.g. radiation- or chemo-therapy) were omitted in responders[52]. No recurrent disease was detected within the responder group during post-operative follow-up visits (>2 years). We compared CT and PET scan images at the time of the diagnosis and post-surgery follow-up examinations. Strikingly, after removal of the tumor and tdLNs, non-tdLNs with clear signs of expansion/reactivity were found in most responders, while non-responders lacked reactive non-tdLNs distant to the initial site of the tumor (**Fig. 7A**). Of note, no metastatic LN involvement was detected in radiology-guided biopsies, indicating that enlarged LNs were indeed immune-reactive. The reactive LNs were higher in the echelon and likely located in new lymph draining routes of the initial tumor site after the removal of the primary tdLNs. For instance, in two patients (#13, #15), lower neck LNs (posterior cervical) and upper neck LNs (submandibular and submental) were enlarged during the follow-up while unremarkable at the time of diagnosis (**Fig. 7C**). Similarly, neck draining mediastinal LNs above the aortic arch in patient #9 were normal at the time of the diagnoses but appeared reactive in CT and PET scans 7-month after tumor and tdLN dissection (**Fig. 7D**). These data suggest that surgical removal of the tdLNs results in a compensatory mechanism that includes antigen diversion to non-tdLNs that extends ICB response in cancer patients.

Discussion

TdLNs are located along the lymphatic drainage pathway of primary tumors with the highest concentration of tumor-derived antigens, which renders them the primary sites to initiate and sustain tumor-specific T cell responses[16,53,54]. Patients with melanoma from a phase II clinical trial with neoadjuvant-adjuvant anti-PD1 (pembrolizumab) treatment had improved event-free survival compared to the adjuvant-only setting[46], indicating that using the primary tumor as the source of antigen and the tdLNs for tumor-specific T cell priming before primary tumor resection is more effective in establishing ICB responses. Recent studies advocate that tdLNs are indispensable for acute and T memory-driven lasting ICB responses[24,25,31]. However, there is data demonstrating that patients still benefit from ICB treatment after sentinel LN and bulky disease-related LN removal[32,55–57], which is in line with our retrospective analysis of stage III melanoma patients (**Fig. 1**). Collectively, these data demonstrate that patients benefited from adjuvant ICB with no detrimental effect of tdLN removal surgery. Recent work from our lab and others has shown that metastatic tdLNs are immune suppressed and can impair systemic anti-cancer immune responses[13–16]. Ultimately, the metastatic burden in tdLNs may determine whether SLNB or CLND has a positive, negative or neutral effect on disease recurrence and survival. As human LN chains are complex with multiple echelons[58], they determine early metastatic involvement and immune activation or suppression status of the sentinel LNs and LNs further downstream. When dissection of metastatic LNs—which are likely to be severely immunosuppressed[59] and restricted in their ability to mount effective T cell responses[60]—is performed, the net benefit of removing these immune suppressive LNs is likely to outweigh any marginal decrease in systemic response to ICB. Based on the local microenvironment experienced by individual LNs—including the presence of metastatic cancer cells, abundance of cancer antigen and immunosuppressive cytokines—different tdLNs can be expected to have different capacities to mount immune responses and maintain responses to ICB. It is key to identify LNs with sufficient exposure to antigen and efficient antigen presentation without immune suppression to target for immunotherapy delivery.

In this study, we emphasize the dynamic and adaptive aspects of antigen transport. Disruption of normal lymphatic drainage diverts migratory dendritic cells and lymph fluid with antigens to adjacent lymphosomes and induces immune responses in non-tdLNs. These LNs can be relatively distant from the original tdLNs, which seems to be counterintuitive but is corroborated by clinical observations[39,61] (**Fig. 7)**. It is likely that the initial amount/concentration of tumor-derived antigen is critical for the maximal transport distance to still meet a threshold for effective immune activation in distant LNs. Long distance transport goes along with antigen dilution and degradation and might fail to induce an inflammatory milieu in LNs that is required for proper T cell priming. Understanding these spatial limits might explain the anatomical distribution of LNs throughout the body to provide effective regional immune surveillance. Intriguingly, we found that CLND in mice induces tumor-specific T cell enrichment in non-tdLNs with ICB treatment, when performed along with primary tumor resection (adjuvant setting). The antigen source fueling the tumor-specific T cell response in distant LNs after primary tumor resection is unknown. Conceivably, surgery might release a larger amount of antigen. Residual tumor cells from the primary site or metastases in distant organs can also contribute to the antigen abundance. Despite the importance of antigen transport to distant LNs, direct T cell priming in the local tumor microenvironment[62] and tertiary lymphoid structures[63] may also contribute to the residual ICB response.

Our findings suggest that long-term anti-tumor immune memory is not predominantly reliant on T cell egress from LNs. It is possible that tumor-specific memory T cells leave the tdLNs after initial activation and reside in tissues until getting reactivated during tumor regrowth or metastasis. Our neoadjuvant-adjuvant ICB study demonstrated that mice that underwent curative surgery retained tumor-specific systemic immune memory, suggesting that adjuvant ICB may act through existing anti-tumor tissue-resident memory T cells.

In our work, surgery of skin LNs in mice was used to recapitulate SLNB and CLND procedures used in the clinic. However, the length scale and anatomical differences are obvious between humans and mice (**Fig. 4)**. Compared to simple chains of a few LNs in a drainage path of mice, humans have more complex and interconnected lymphatic networks with multiple LNs draining the same lymphosome[58], so that the removal of a single LN in mice resembles CLND in humans. Consistent with our preclinical data, compensatory lymphatic drainage[39,61], even in the presence of lymphedema[37–39,61], and distant LN activation are observed in cancer patients (**Fig. 7)**. In future work, it will be of interest to investigate lymphatic drainage patterns apart from the lymphatic network of the skin, as ICB treatment also increases survival in non-small cell lung cancer[64] and colorectal cancer[65], which may have less access to adjacent lymphosomes to access alternative LNs. Our data present a better understanding of the challenges associated with integrating ICB therapy into clinical practice in patients undergoing LN resections. It is critical to continue to advance this understanding to improve ICB responses in patients with metastatic cancer.

Figures

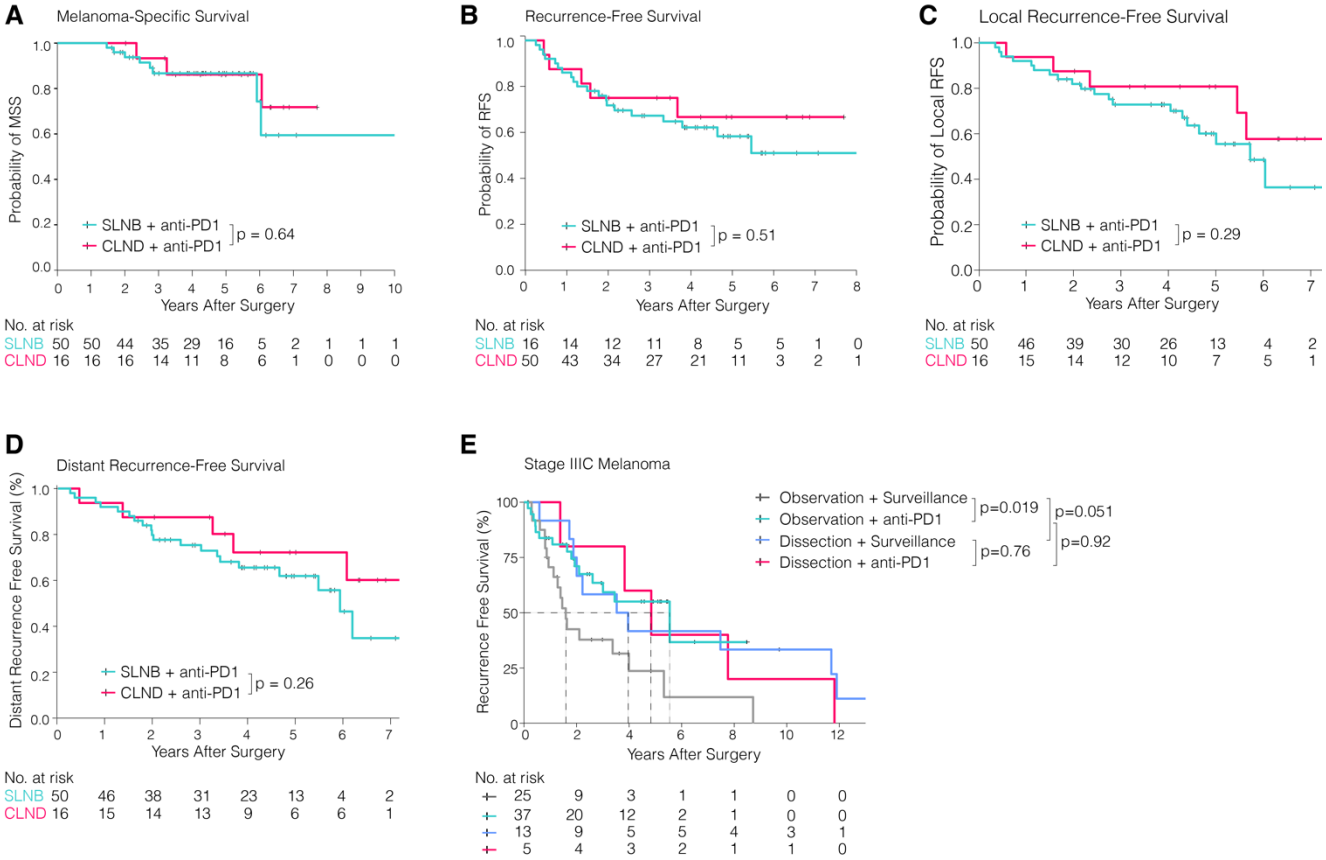

Figure 1. Adjuvant ICB response persists in stage III melanoma patients after LN surgery. Retrospective analysis with a cohort of cutaneous stage III melanoma patients who underwent SLNB or CLND, treated with adjuvant anti-PD1 antibody (nivolumab or pembrolizumab) at the Massachusetts General Hospital. (**A)** Melanoma-specific survival, (**B)** recurrence-free survival, **(C)** local recurrence-free survival and **(D)** distant recurrence-free survival. (**E)** Retrospective analysis of stage IIIC melanoma patients with observation or LN dissection and either surveillance or anti-PD1 treatment. Statistical analysis with Log-rank test.

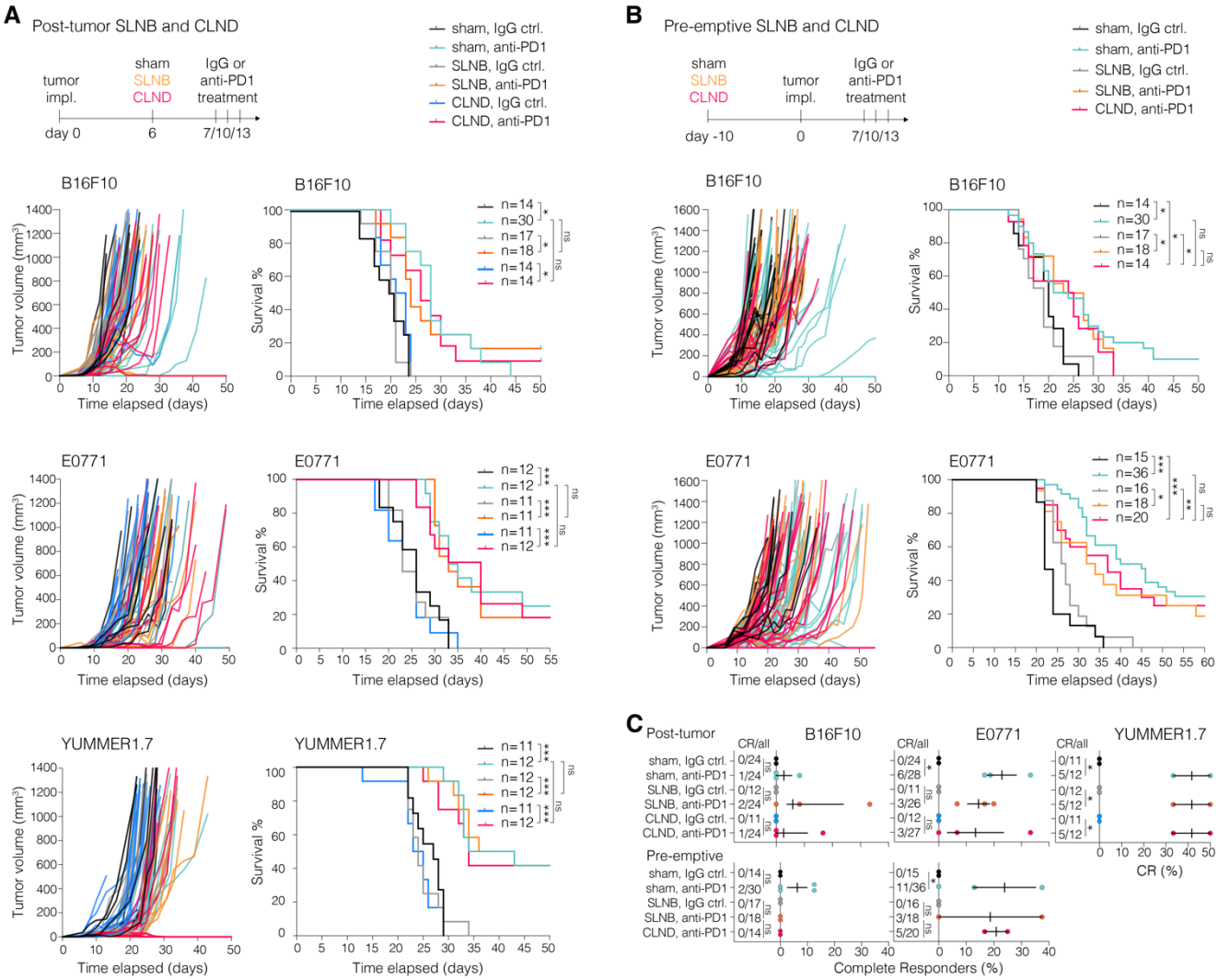

Figure 2. ICB response persists after LN dissection. (A) Orthotopically implanted B16F10, E0771 or YUMMER1.7 tumors in mice with sham surgery, SLNB, or CLND and IgG control or anti-PD1 treatment. **(B)** Pre-emptive sham surgery, SLNB, or CLND and orthotopic B16F10 or E0771 tumor implantation. **(C)** Data points represent the average percentage of complete responders per experiment. Complete responders (CR) as a fraction of the total number of mice are indicated as CR/all. Number of mice per group indicated as n from 2-3 individual experiments. Statistical analysis with Log-rank test (A,B) or Fisher's exact test (C), ns=not significant *p<0.05, **p<0.01, ***p<0.005.

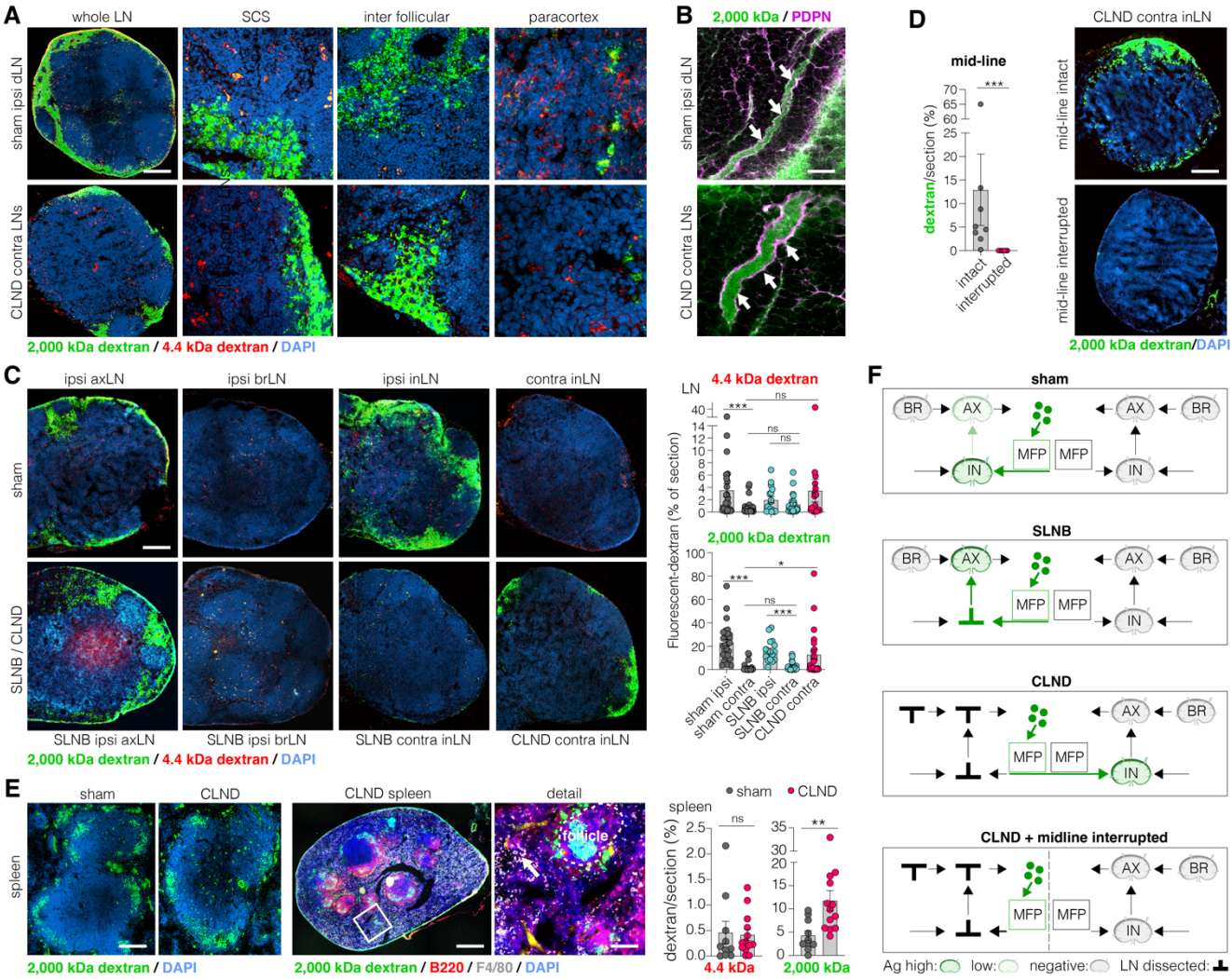

Figure 3. Dissection of draining LNs promotes antigen transport to distant LNs. (A) Representative images demonstrate intranodal dextran distribution on the ipsilateral side after sham surgery or contralateral side after CLND. Subcapsular sinus (SCS). Scale bar: 500 µm. **(B)** Representative images of 2,000 kDa FITC-dextran within lymphatic vessels (Podoplanin, PDPN) in LNs of the different groups, respectively. **(C)** 2,000 kDa FITC-dextran and 4.4 kDa TRITC-dextran were injected into the mammary fat pad (MFP) after sham surgery, SLNB or CLND. Dextran distribution 6 hours post-injection in axillary (axLN), brachial (brLN) and inguinal (inLN) LNs after sham, SLNB or CLND. Quantification of the fluorescent area (FITC or TRITC) in percent of whole section. **(D)** 2,000 kDa FITC-dextran in contralateral inLN 6 hours post-injection into the ipsilateral MFP of mice after CLND with intact or interrupted (cut) midline of the ventral skin. **(E)** Representative images and quantification of 2,000 kDa FITC-dextran in spleen of mice after sham surgery or CLND with immunostaining for B cells (B220) and macrophages (F4/80). **(F)** Illustration of lymph flow patterns during different surgery settings. Scale bars: 500 µm (A, C, D, E), 100 µm (B, E detail). Graphs show mean ± SEM with data points representing individual animals. Statistical analysis with Mann-Whitney U test (B, E, F), ns= not significant, *p<0.05, **p<0.01, ***p<0.005.

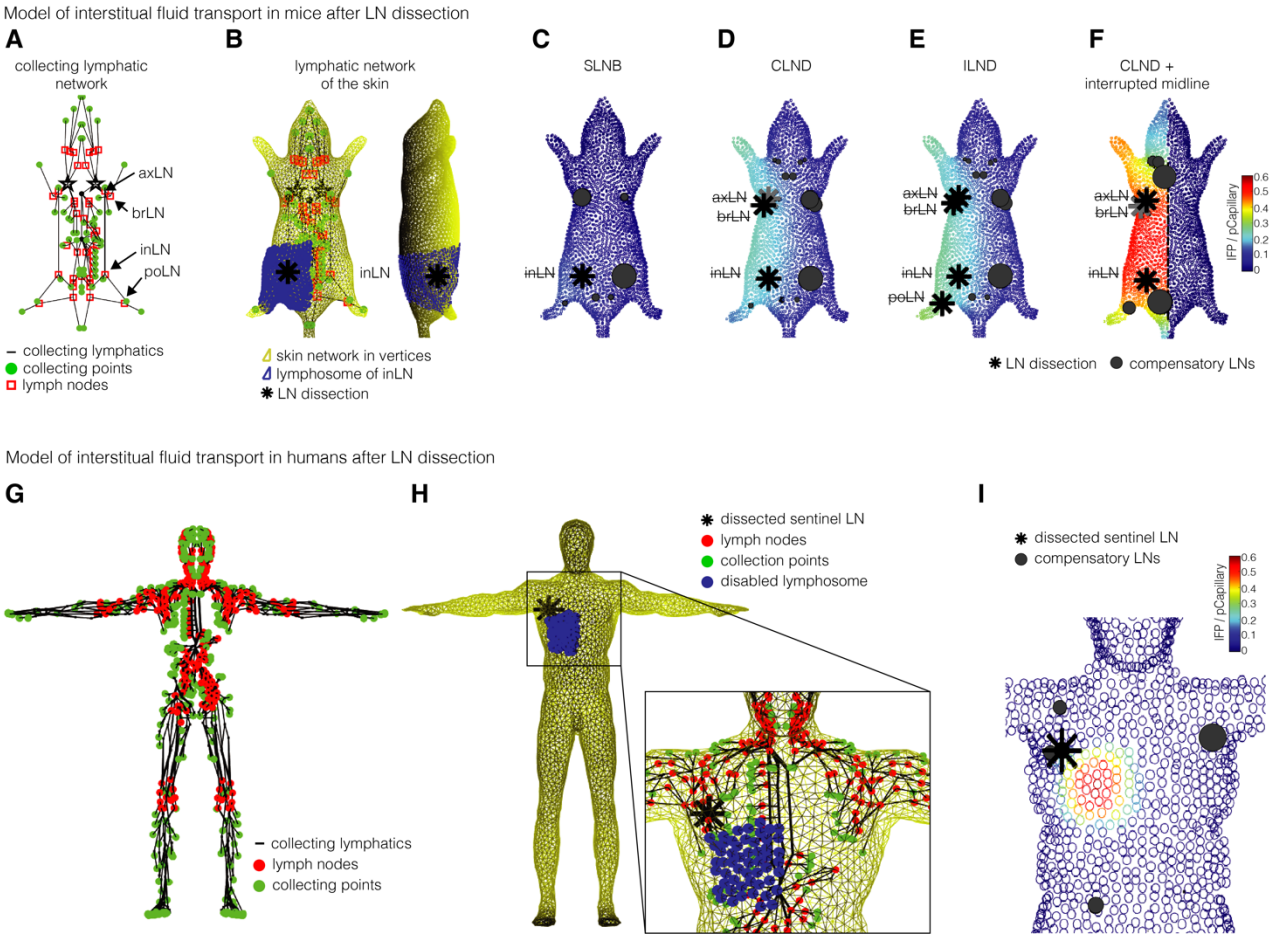

Figure 4. Mathematical modeling of antigen access to adjacent lymphosomes via dermal transport after node dissection. (A) Mouse model with the network of collecting lymphatic vessels (black), collecting points (blue) and lymph nodes (red). **(B)** Computational mesh (yellow) for the network of initial lymphatic vessels in the skin showing the drainage basin (lymphosome) (blue) for the right inguinal node (*). (**C-F)** Color maps of the interstitial pressure relative to the capillary blood pressure for disabled nodes (*) [(**c**) SLNB (inLN), (**D**) CLND (in/ax/br), (**E**) ILND (po/in/ax/br), (**F)** CLND (in/ax/br) with severed midline]. The dark circles represent compensatory lymph nodes and are scaled by the fraction of diverted flow they must carry. **(G)** Human male model with the network of collecting lymphatic vessels (black), collecting points (blue) and lymph nodes (red). **(H)** Computational mesh (yellow) for the network of initial lymphatic vessels in the skin showing the drainage basin lymphosome (blue) for a right axillary node (*). **I)** Color map of the interstitial pressure relative to the capillary blood pressure for a disabled right axillary node (*) with dark circles representing the compensatory lymph nodes scaled by the change in flow induced by the diversion of flow from the disabled lymphosome.

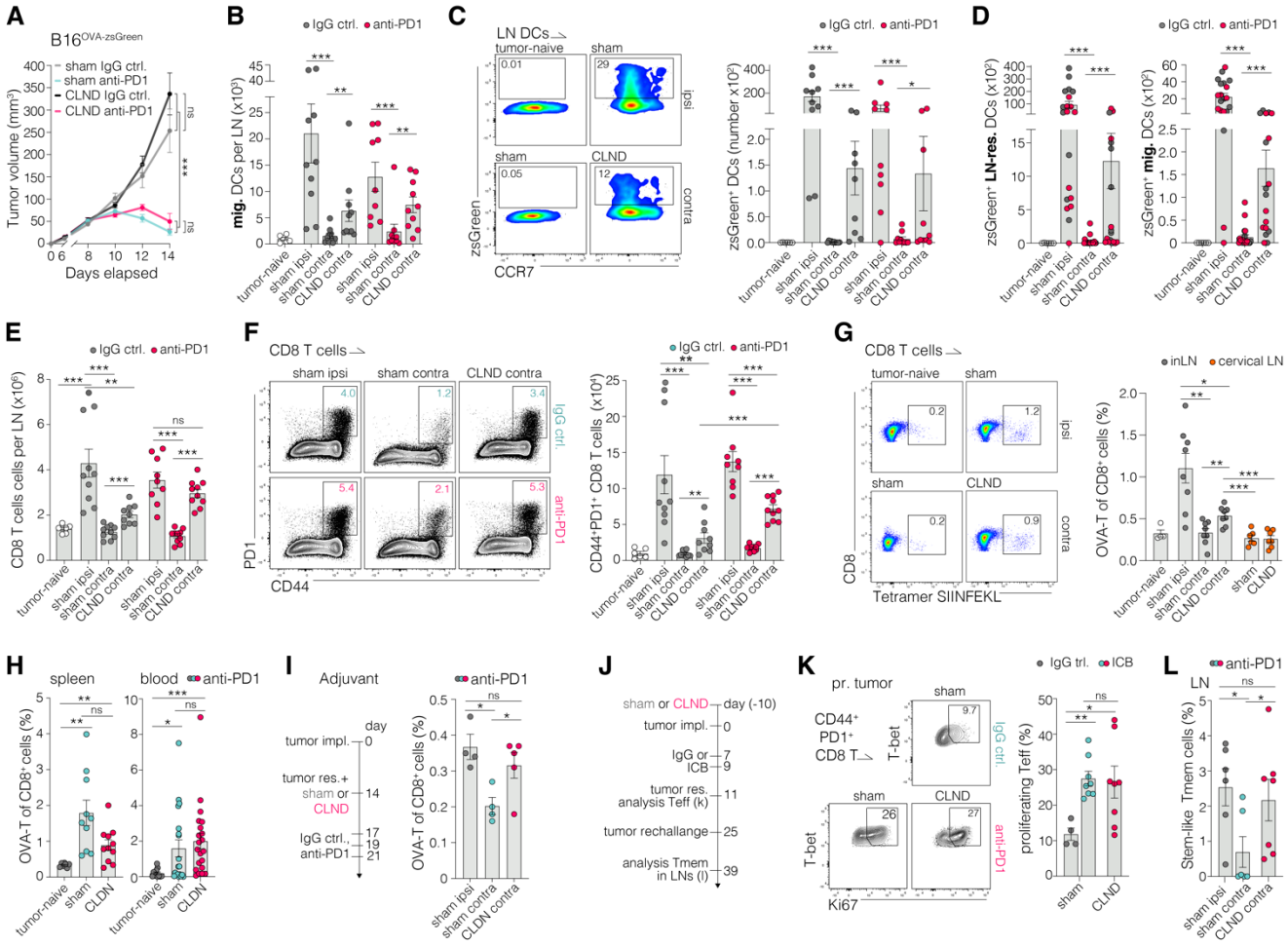

Figure 5. T cell responses arise in distant LNs after ipsilateral CLND. (A) Volume of B16$^{OVA\text{-}zsGreen}$ tumors, n=11-12 per group in 2 individual experiments. Corresponding to flow analysis in B, C, D, E, F. Experimental set up illustrated in Figure S5A. **(B)** Number of migratory DCs per LN, analyzed by flow cytometry, gating strategy in Figure S5b. **(C)** Representative flow cytometry plots and quantification of the number of zsGreen^{+} DCs per LN. **(D)** Number of zsGreen^{+} migratory and LN-resident DCs. **(E)** Number of CD8 T cells in LNs of mice with B16$^{OVA\text{-}zsGreen}$ tumor. **(F)** Representative flow cytometry plots and number of antigen-experienced (CD44^{+}PD1^{+}) CD8 T cells per LN. Tetramer^{+} (MHCI-SIINFEKL) CD8 cells in **(G)** LNs, and **h)** spleen and blood of mice with B16^{OVA} tumors. **(I)** Frequency of OVA-specific CD8 T cells in LNs in an adjuvant setting with primary tumor resection combined with CLND and anti-PD1 treatment. **(J)** Experimental set up to analyze effector T cells (Teff) in the primary tumor and memory T cells (Tmem) in LNs after tumor rechallenge. Corresponding to K, L. **(K)** CD8 effector T cells within the primary tumor, gating strategy in Figure S6a. **(L)** Stem-like T memory cells in LNs of mice after tumor rechallenge, gating strategy in Figure S6b. Graphs show mean ± SEM, data points representing individual animals. Statistical analysis with Mann-Whitney U test (B, C, D, E, F, G, H, K, L), t-test (I) or 2-way ANOVA (A), ns= not significant, *p<0.05, **p<0.01, ***p<0.005.

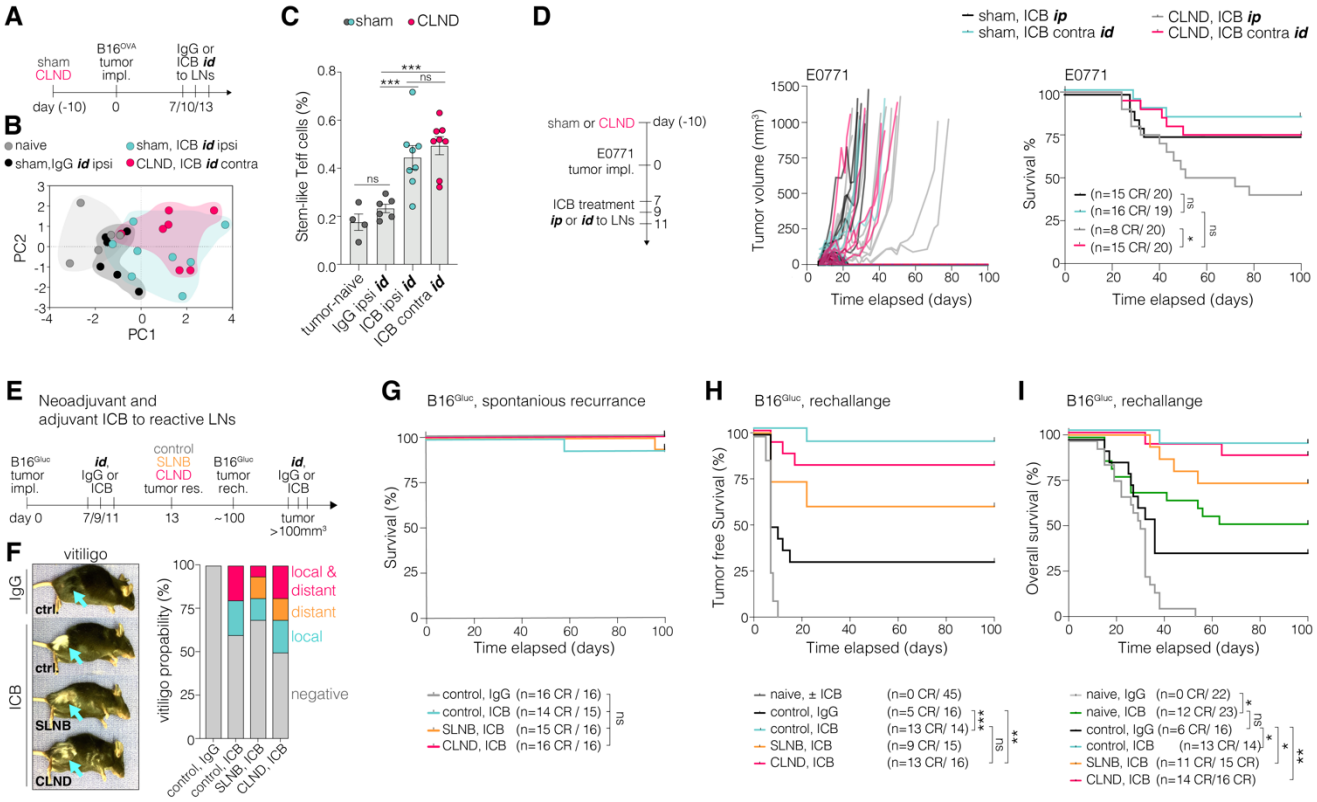

Figure 6. Administration of ICB to distant LNs improves response after CLND. (A) Experimental set up, pre-emptive sham surgery or CLND before orthotopic E0771 tumor implantation. IgG control or a combination of anti-PD1 and anti-CTLA4 were intradermally (*id*) administered to the ipsilateral LNs or contralateral LNs (referred to as ICB). Corresponding to b,c. **(B)** Principal component analysis of T cells from respective LNs. Analysis based on the abundance of antigen-experienced T cells ($CD44^+$, $PD1^+$), stem-like T cells ($CD44^+$, $PD1^+$, $TCF1^+$), central memory T cells ($CD44^+$, $CD62L^+$), effector memory T cells ($CD44^+$, $CD62L^-$, $PD1^-$), stem-like effector memory T cells ($CD44^+$, $PD1^+$, $TCF1^+$, $CD62L^-$, $CD39^-$). **(C)** Percentage of stem-like effector memory T cells in all T cells. **(D)** Tumor volume and overall survival of mice with E0771 tumors. Neo-adjuvant ICB was administered *ip* or *id* to the contralateral inLN. n indicates the number of mice per group of at least 2 experiments, complete responders (CR). **(E)** Experimental set up of neoadjuvant-adjuvant treatment of E0771 and tumor rechallenge. Control group represents tumor resection without LN surgery. **(F)** Representative images of vitiligo (arrows) that developed in mice after neoadjuvant treatment and quantification of mice with local, distant or local and distant vitiligo relative to the side of tumor implantation. Corresponding to F, G, H, I. **(G)** Overall survival during spontaneous tumor recurrence. **H)** Tumor-free survival of mice previously treated with neoadjuvant ICB, primary tumor resection and tumor rechallenge. Naïve and untreated mice were used as controls for tumor rechallenge. **(I)** Overall survival of mice treated with neoadjuvant-adjuvant ICB after the rechallenge. n indicates the number of mice per group of at least 2 experiments. Graphs show mean ± SEM with data points representing individual animals. Statistical analysis with Mann-Whitney U test (C) or Log-rank test (D, G, H, I), ns= not significant, *p<0.05, **p<0.01, ***p<0.005.

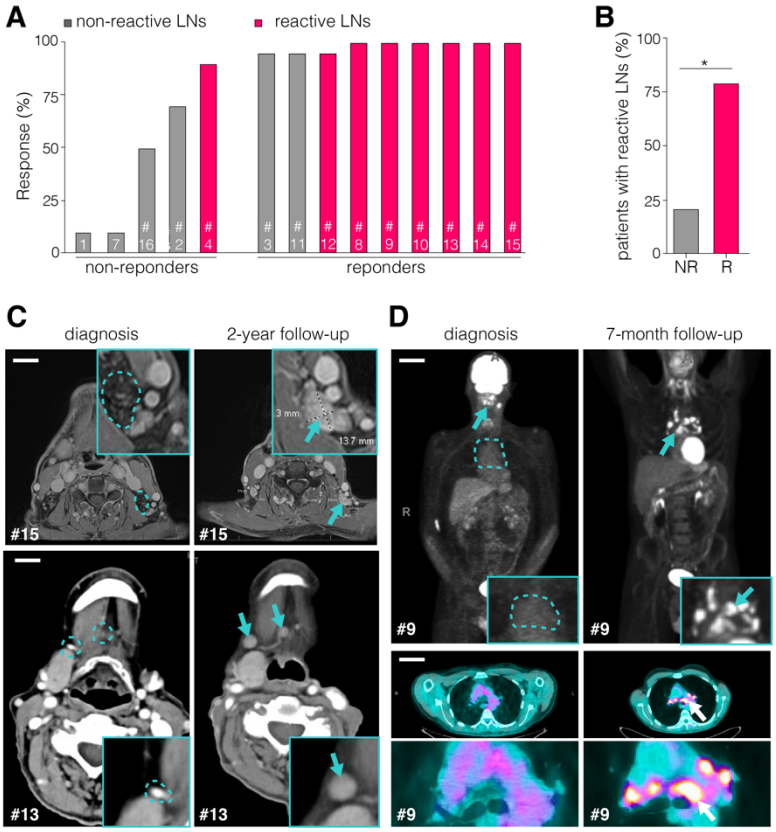

Figure 7. Non-tdLNs become reactive after resection of the primary tumor and related LNs in cancer patients. (A) Response rate and reactive status of remaining LNs after primary tumor and LN dissection in the neck of patients with head and neck cancer. **(B)** Percentage of patients with enlarged or reactive non-tdLNs in more distant LN basins. **(C)** CT scan images of patient #13 and #15 at time point of diagnosis and follow-up 2-years post-surgery. Arrows indicate enlarged neck LNs (posterior cervical LNs in patient #13; submandibular and submental LNs in patient #15). **(D)** CT and PET scan images of patient #9 at diagnosis and at follow-up 7-month post-surgery. Arrows indicate reactive cervical (diagnosis) and apex mediastinal LNs (follow up). All data and images are part of the phase I trial NCT03635164. Statistical analysis performed with Fisher's exact test (B), *p<0.05.

References

1. Ishida, Y., Agata, Y., Shibahara, K. & Honjo, T. Induced expression of PD-1, a novel member of the immunoglobulin gene superfamily, upon programmed cell death. *EMBO J* **11**, 3887–3895 (1992).
2. Iwai, Y. *et al.* Involvement of PD-L1 on tumor cells in the escape from host immune system and tumor immunotherapy by PD-L1 blockade. *Proc Natl Acad Sci U S A* **99**, 12293–12297 (2002).
3. Brunet, J.-F. *et al.* A new member of the immunoglobulin superfamily—CTLA-4. *Nature* **328**, 267–270 (1987).
4. Leach, D. R., Krummel, M. F. & Allison, J. P. Enhancement of antitumor immunity by CTLA-4 blockade. *Science* **271**, 1734–1736 (1996).
5. Hargadon, K. M., Johnson, C. E. & Williams, C. J. Immune checkpoint blockade therapy for cancer: An overview of FDA-approved immune checkpoint inhibitors. *Int Immunopharmacol* **62**, 29–39 (2018).
6. Wei, S. C., Duffy, C. R. & Allison, J. P. Fundamental Mechanisms of Immune Checkpoint Blockade Therapy. *Cancer Discov* **8**, 1069–1086 (2018).
7. Hodi, F. S. *et al.* Improved survival with ipilimumab in patients with metastatic melanoma. *N Engl J Med* **363**, 711–723 (2010).
8. Robert, C. *et al.* Nivolumab in previously untreated melanoma without BRAF mutation. *N Engl J Med* **372**, 320–330 (2015).
9. Schmid, P. *et al.* Pembrolizumab for Early Triple-Negative Breast Cancer. *N Engl J Med* **382**, 810–821 (2020).
10. Cortes, J. *et al.* Pembrolizumab plus Chemotherapy in Advanced Triple-Negative Breast Cancer. *N Engl J Med* **387**, 217–226 (2022).
11. Padera, T. P., Meijer, E. F. J. & Munn, L. L. The Lymphatic System in Disease Processes and Cancer Progression. *Annu Rev Biomed Eng* **18**, 125–158 (2016).
12. Zhou, H., Lei, P.-J. & Padera, T. P. Progression of Metastasis through Lymphatic System. *Cells* **10**, 627 (2021).
13. Jones, D. *et al.* Solid stress impairs lymphocyte infiltration into lymph-node metastases. *Nat Biomed Eng* **5**, 1426–1436 (2021).
14. Lei, P.-J. *et al.* Cancer cell plasticity and MHC-II-mediated immune tolerance promote breast cancer metastasis to lymph nodes. *J Exp Med* **220**, e20221847 (2023).
15. Reticker-Flynn, N. E. *et al.* Lymph node colonization induces tumor-immune tolerance to promote distant metastasis. *Cell* **185**, 1924-1942.e23 (2022).
16. Núñez, N. G. *et al.* Tumor invasion in draining lymph nodes is associated with Treg accumulation in breast cancer patients. *Nat Commun* **11**, 3272 (2020).
17. Brown, M. *et al.* Lymph node blood vessels provide exit routes for metastatic tumor cell dissemination in mice. *Science* **359**, 1408–1411 (2018).
18. Pereira, E. R. *et al.* Lymph node metastases can invade local blood vessels, exit the node, and colonize distant organs in mice. *Science* **359**, 1403–1407 (2018).
19. Alatengbaolide, null *et al.* Lymph node ratio is an independent prognostic factor in gastric cancer after curative resection (R0) regardless of the examined number of lymph nodes. *Am J Clin Oncol* **36**, 325–330 (2013).
20. Aoyama, T. *et al.* The Lymph Node Ratio Is an Independent Prognostic Factor in Pancreatic Cancer Patients Who Receive Curative Resection Followed by Adjuvant Chemotherapy. *Anticancer Res* **38**, 4877–4882 (2018).
21. Chen, C.-C., Lin, J.-C. & Chen, K.-W. Lymph node ratio as a prognostic factor in head and neck cancer patients. *Radiat Oncol* **10**, 181 (2015).
22. Scoggins, C. R. *et al.* Prognostic information from sentinel lymph node biopsy in patients with thick melanoma. *Arch Surg* **145**, 622–627 (2010).
23. Voordeckers, M., Vinh-Hung, V., Van de Steene, J., Lamote, J. & Storme, G. The lymph node ratio as prognostic factor in node-positive breast cancer. *Radiother Oncol* **70**, 225–230 (2004).
24. Dammeijer, F. *et al.* The PD-1/PD-L1-Checkpoint Restrains T cell Immunity in Tumor-Draining Lymph Nodes. *Cancer Cell* **38**, 685-700.e8 (2020).
25. Huang, Q. *et al.* The primordial differentiation of tumor-specific memory CD8+ T cells as bona fide responders to PD-1/PD-L1 blockade in draining lymph nodes. *Cell* **185**, 4049-4066.e25 (2022).
26. Eggermont, A. M. M. *et al.* Adjuvant ipilimumab versus placebo after complete resection of high-risk stage III melanoma (EORTC 18071): a randomised, double-blind, phase 3 trial. *Lancet Oncol* **16**, 522–530 (2015).
27. van Pul, K. M. *et al.* Local delivery of low-dose anti-CTLA-4 to the melanoma lymphatic basin leads to systemic Treg reduction and effector T cell activation. *Sci Immunol* **7**, eabn8097 (2022).
28. Faries, M. B. *et al.* Completion Dissection or Observation for Sentinel-Node Metastasis in Melanoma. *N Engl J Med* **376**, 2211–2222 (2017).

29. Fransen, M. F. *et al.* Tumor-draining lymph nodes are pivotal in PD-1/PD-L1 checkpoint therapy. *JCI Insight* **3**, (2018).
30. Zhao, X., Kassaye, B., Wangmo, D., Lou, E. & Subramanian, S. Chemotherapy but Not the Tumor Draining Lymph Nodes Determine the Immunotherapy Response in Secondary Tumors. *iScience* **23**, 101056 (2020).
31. Yang, H. *et al.* Multi-scale characterization of tumor-draining lymph nodes in resectable lung cancer treated with neoadjuvant immune checkpoint inhibitors. *eBioMedicine* **84**, (2022).
32. Ogata, D. *et al.* Effect of lymph node dissection and adjuvant therapy in patients with sentinel node+ melanoma: An observational multicenter study. *JCO* **41**, e21569–e21569 (2023).
33. De Togni, P. *et al.* Abnormal development of peripheral lymphoid organs in mice deficient in lymphotoxin. *Science* **264**, 703–707 (1994).
34. Banks, T. A. *et al.* Lymphotoxin-alpha-deficient mice. Effects on secondary lymphoid organ development and humoral immune responsiveness. *J Immunol* **155**, 1685–1693 (1995).
35. Mariathasan, S. *et al.* Absence of lymph nodes in lymphotoxin-alpha(LT alpha)-deficient mice is due to abnormal organ development, not defective lymphocyte migration. *J Inflamm* **45**, 72–78 (1995).
36. Rantakari, P. *et al.* The endothelial protein PLVAP in lymphatics controls the entry of lymphocytes and antigens into lymph nodes. *Nat Immunol* **16**, 386–396 (2015).
37. Heydon-White, A., Suami, H., Boyages, J., Koelmeyer, L. & Peebles, K. C. Assessing breast lymphoedema following breast cancer treatment using indocyanine green lymphography. *Breast Cancer Res Treat* **181**, 635–644 (2020).
38. Suami, H. *et al.* A new indocyanine green fluorescence lymphography protocol for diagnostic assessment of lower limb lymphoedema. *J Plast Reconstr Aesthet Surg* **75**, 3946–3955 (2022).
39. Maaskant-Braat, A. J. G. *et al.* Lymphatic mapping after previous breast surgery. *Breast* **21**, 444–448 (2012).
40. Gerner, M. Y., Torabi-Parizi, P. & Germain, R. N. Strategically Localized Dendritic Cells Promote Rapid T Cell Responses to Lymph-Borne Particulate Antigens. *Immunity* **42**, 172–185 (2015).
41. Francis, D. M. *et al.* Blockade of immune checkpoints in lymph nodes through locoregional delivery augments cancer immunotherapy. *Sci Transl Med* **12**, eaay3575 (2020).
42. O'Melia, M. J., Manspeaker, M. P. & Thomas, S. N. Tumor-draining lymph nodes are survival niches that support T cell priming against lymphatic transported tumor antigen and effects of immune checkpoint blockade in TNBC. *Cancer Immunol Immunother* **70**, 2179–2195 (2021).
43. Buchbinder, E. I. & Desai, A. CTLA-4 and PD-1 Pathways: Similarities, Differences, and Implications of Their Inhibition. *American Journal of Clinical Oncology* **39**, 98 (2016).
44. Wolchok, J. D. *et al.* Long-Term Outcomes With Nivolumab Plus Ipilimumab or Nivolumab Alone Versus Ipilimumab in Patients With Advanced Melanoma. *JCO* **40**, 127–137 (2022).
45. Siddiqui, I. *et al.* Intratumoral Tcf1+PD-1+CD8+ T Cells with Stem-like Properties Promote Tumor Control in Response to Vaccination and Checkpoint Blockade Immunotherapy. *Immunity* **50**, 195-211.e10 (2019).
46. Patel, S. P. *et al.* Neoadjuvant-Adjuvant or Adjuvant-Only Pembrolizumab in Advanced Melanoma. *N Engl J Med* **388**, 813–823 (2023).
47. Lo, J. A. *et al.* Epitope spreading toward wild-type melanocyte-lineage antigens rescues suboptimal immune checkpoint blockade responses. *Science Translational Medicine* **13**, eabd8636 (2021).
48. Baeyens, A., Fang, V., Chen, C. & Schwab, S. R. Exit Strategies: S1P Signaling and T Cell Migration. *Trends Immunol* **36**, 778–787 (2015).
49. Girard, J.-P., Moussion, C. & Förster, R. HEVs, lymphatics and homeostatic immune cell trafficking in lymph nodes. *Nat Rev Immunol* **12**, 762–773 (2012).
50. Cyster, J. G. & Schwab, S. R. Sphingosine-1-phosphate and lymphocyte egress from lymphoid organs. *Annu Rev Immunol* **30**, 69–94 (2012).
51. Brinkmann, V., Cyster, J. G. & Hla, T. FTY720: sphingosine 1-phosphate receptor-1 in the control of lymphocyte egress and endothelial barrier function. *Am J Transplant* **4**, 1019–1025 (2004).
52. Darragh, L. B. *et al.* A phase I/Ib trial and biological correlate analysis of neoadjuvant SBRT with single-dose durvalumab in HPV-unrelated locally advanced HNSCC. *Nat Cancer* **3**, 1300–1317 (2022).
53. Delclaux, I., Ventre, K. S., Jones, D. & Lund, A. W. The tumor-draining lymph node as a reservoir for systemic immune surveillance. *Trends in Cancer* **10**, 28–37 (2024).
54. Li, Z. *et al.* In vivo labeling reveals continuous trafficking of TCF-1+ T cells between tumor and lymphoid tissue. *J Exp Med* **219**, e20210749 (2022).
55. Weber, J. *et al.* Adjuvant Nivolumab versus Ipilimumab in Resected Stage III or IV Melanoma. *N Engl J Med* **377**, 1824–1835 (2017).
56. Ascierto, P. A. *et al.* Adjuvant nivolumab versus ipilimumab in resected stage IIIB-C and stage IV melanoma (CheckMate 238): 4-year results from a multicentre, double-blind, randomised, controlled, phase 3 trial. *Lancet Oncol* **21**, 1465–1477 (2020).

57. Weber, J. S. *et al.* Adjuvant Therapy of Nivolumab Combined With Ipilimumab Versus Nivolumab Alone in Patients With Resected Stage IIIB-D or Stage IV Melanoma (CheckMate 915). *J Clin Oncol* **41**, 517–527 (2023).
58. Haley, P. J. The lymphoid system: a review of species differences. *J Toxicol Pathol* **30**, 111–123 (2017).
59. Jones, D., Pereira, E. R. & Padera, T. P. Growth and Immune Evasion of Lymph Node Metastasis. *Front Oncol* **8**, 36 (2018).
60. Rahim, M. K. *et al.* Dynamic CD8+ T cell responses to cancer immunotherapy in human regional lymph nodes are disrupted in metastatic lymph nodes. *Cell* **186**, 1127-1143.e18 (2023).
61. Sato, A. *et al.* Altered lymphatic drainage patterns in re-operative sentinel lymph node biopsy for ipsilateral breast tumor recurrence. *Radiat Oncol* **14**, 159 (2019).
62. Fu, C. & Jiang, A. Dendritic Cells and CD8 T Cell Immunity in Tumor Microenvironment. *Front Immunol* **9**, 3059 (2018).
63. Bery, A. I. *et al.* Role of tertiary lymphoid organs in the regulation of immune responses in the periphery. *Cell Mol Life Sci* **79**, 359 (2022).
64. Onoi, K. *et al.* Immune Checkpoint Inhibitors for Lung Cancer Treatment: A Review. *J Clin Med* **9**, 1362 (2020).
65. Boukouris, A. E. *et al.* Latest evidence on immune checkpoint inhibitors in metastatic colorectal cancer: A 2022 update. *Crit Rev Oncol Hematol* **173**, 103663 (2022).
66. Savinkov, R. *et al.* Graph Theory for Modeling and Analysis of the Human Lymphatic System. *Mathematics* **8**, 2236 (2020).
67. Grebennikov, D., Savinkov, R., Zelenova, E., Lobov, G. & Bocharov, G. Network Modeling of Murine Lymphatic System. *Algorithms* **16**, 168 (2023).
68. Kawashima, Y., Sugimura, M., Hwang, Y.-C. & Kudo, N. THE LYMPH SYSTEM IN MICE. *Japanese Journal of Veterinary Research* **12**, 69–78 (1964).
69. Van Den Broeck, W., Derore, A. & Simoens, P. Anatomy and nomenclature of murine lymph nodes: Descriptive study and nomenclatory standardization in BALB/cAnNCrl mice. *Journal of Immunological Methods* **312**, 12–19 (2006).
70. Harrell, M. I., Iritani, B. M. & Ruddell, A. Lymph node mapping in the mouse. *J Immunol Methods* **332**, 170–174 (2008).
71. Suami, H. & Scaglioni, M. F. Lymphatic Territories (Lymphosomes) in the Rat: An Anatomical Study for Future Lymphatic Research. *Plast Reconstr Surg* **140**, 945–951 (2017).
72. Baxter, L. T. & Jain, R. K. Transport of fluid and macromolecules in tumors. I. Role of interstitial pressure and convection. *Microvasc Res* **37**, 77–104 (1989).
73. Swartz, M. A. *et al.* Mechanics of interstitial-lymphatic fluid transport: theoretical foundation and experimental validation. *Journal of Biomechanics* **32**, 1297–1307 (1999).
74. Truskey, G. A., Yuan, F. & Katz, D. F. *Transport Phenomena in Biological Systems*. (Prentice Hall, 2009).

ACKNOWLEDGEMENTS

Funding:

The Rullo Family MGH Research Scholar Award (T.P.P.)

Emma and Bill Roberts MGH Research Scholar Award (G.M.B.)

National Institutes of Health grant K00CA234940 (H.Z.)

National Institutes of Health grant R21AG072205 (T.P.P.)

National Institutes of Health grant R01CA214913 (T.P.P.)

National Institutes of Health grant R01HL128168 (T.P.P.)

National Institutes of Health grant R01CA284372 (T.P.P.)

National Institutes of Health grant R01CA284603 (T.P.P., L.L.M. and J.W.B.)

National Institutes of Health grant R01DE028529 (S.D.K.)

National Institutes of Health grant R01DE028282 (S.D.K.)

National Institutes of Health grant P50CA261605 (S.D.K.)

National Institutes of Health grant R35CA242379 (M.G.V.H.)

The Bridge Project, a partnership between the Koch Institute for Integrative Cancer Research at MIT and the Dana-Farber/Harvard Cancer Center (T.P.P., M.G.V.H.)

The Patricia K. Donahoe Award from the Huiying Foundation (G.M.B.)

The Adelson Medical Research Foundation (G.M.B.),

The Ludwig Center at MIT (M.G.V.H.)

The MIT Center for Precision Cancer Medicine (M.G.V.H.)

The Breast Cancer Alliance (J.M.U.)

The Melanoma Research Foundation (J.M.U.).

Deutsche Forschungsgemeinschaft ME5486/1-2 (L.M.)

Competing Interests:

H.Z. acknowledges that he is a scientific advisor for AOA dx. M.G.V.H. acknowledges that he is a scientific advisor for Agios Pharmaceuticals, iTeos Therapeutics, Sage Therapeutics, Pretzel Therapeutics, Lime Therapeutics, Auron Therapeutics, and Droia Ventures. G.M.B has sponsored research agreements through her institution with: Olink Proteomics, Teiko Bio, InterVenn Biosciences, Palleon Pharmaceuticals. She served on advisory boards for: Iovance, Merck, Nektar Therapeutics, Novartis, and Ankyra Therapeutics. She consults for: Merck, InterVenn Biosciences, Iovance, and Ankyra Therapeutics. She holds equity in Ankyra Therapeutics. The Phase I/Ib clinical trial NCT03635164 was funded by AstraZeneca, S.D.K also received clinical trial funding from Genentech and preclinical funding from Roche.

Author Contributions:

Conceptualization: H.Z., J.W.B., M.G.V.H., L.L.M., G.M.B., S.C., S.D.K., T.P.P.

Methodology: H.Z., L.M., J.W.B., M.G.V.H., L.L.M., G.M.B., S.C., S.D.K., T.P.P.

Data acquisition: H.Z., L.M., J.W.B., M.J.O., L.B.D., E.S., J.C., P.J.L., J.J.R.

Intellectual input: H.Z., L.M., J.W.B., M.J.O., P.J.L., M.R.N., M.S.R., M.G.V.H., J.M.U., L.L.M., G.M.B., S.C., S.D.K., T.P.P.

Project administration: H.Z., T.P.P.

Supervision: G.M.B., S.C., S.D.K., M.G.V.H., T.P.P.

Writing: H.Z., L.M., J.W.B., M.J.O., P.J.L., M.G.V.H., J.M.U., L.L.M., G.M.B., S.C., S.D.K., T.P.P.